J. Fluid Mech. (1975), *vol.* 68, *part* 4, *pp.* 801–812
Printed in Great Britain

The steady streaming induced by a vibrating cylinder

By N. RILEY

School of Mathematics and Physics, University of East Anglia,
Norwich, England

(Received 16 August 1974 and in revised form 8 November 1974)

In this paper we apply the techniques of higher-order boundary-layer theory to study the steady streaming induced in the neighbourhood of a cylinder which vibrates harmonically, perpendicular to its generators, in an unbounded fluid. The theoretical predictions are compared with the results of experiments performed at high streaming Reynolds numbers. Improved agreement between theory and experiment is achieved although unresolved discrepancies remain.

1. Introduction

When a body, of typical dimension a, performs small amplitude vibrations with speed $U_\infty \cos \omega t'$ in a fluid, of kinematic viscosity ν, which is otherwise at rest then a non-zero mean flow, or steady streaming, is induced in addition to the oscillatory flow components (Longuet-Higgins 1953; Stuart 1963, 1966; Riley 1965, 1967; Davidson & Riley 1972). If the viscous length $(\nu/\omega)^{\frac{1}{2}} \ll a$ then this steady streaming arises directly from the action of Reynolds stresses within the Stokes shear layer, where the induced mean velocities are $O(\epsilon U_\infty)$ with $\epsilon = U_\infty/\omega a \ll 1$. This streaming motion persists outside the shear layer and has been the subject of recent research by the aforementioned authors. Thus Stuart (1963) argued that with streaming velocities $O(\epsilon U_\infty)$ the mean motion outside the Stokes layer will be characterized by the parameter

$$R_s = \epsilon U_\infty a/\nu = U_\infty^2/\omega\nu,$$

which fulfils the role of a Reynolds number. For $R_s \gg 1$ the outer mean flow assumes a boundary-layer character; Stuart (1966) and Riley (1965) developed series solutions for this outer boundary-layer flow starting at the stagnation points S shown in figure 1, where the cylinder is assumed to have a circular cross-section. Stuart conjectured that this outer boundary layer will maintain its identity up to the point C, resulting in a 'collision' of the boundary layers leading, in turn, to the development of a jet-like flow along the axis of oscillation as shown in figure 1. Davidson & Riley (1972) have confirmed experimentally the existence of this jet-like flow and have extended the series solutions by integrating the boundary-layer equations numerically between S and C (figure 1). By measuring the momentum flux in the jet and relating this to the terminal momentum flux in the boundary layer, encouraging agreement was achieved between theory and experiment.

In a recent study Bertelsen (1974) has carried out measurements in the boun-

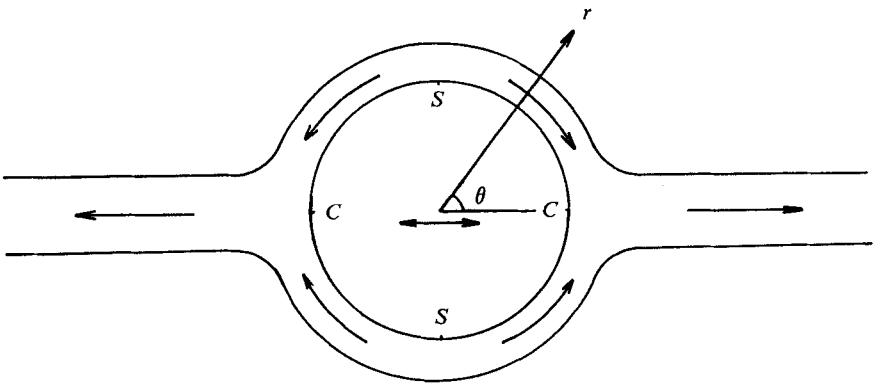

FIGURE 1. Schematic representation of the steady boundary layer and jet induced by the oscillations.

dary layer on a cylinder of circular cross-section, at a location approximately 57° from the point S in figure 1. A brass tube was placed inside a large cylindrical liquid-filled container. The cylinder was supplied with an alternating current and placed in a magnetic field, thus forcing sinusoidal oscillations. Tracer particles were introduced into the liquid and photographed using stroboscopic illumination synchronized to the frequency of the oscillation. From photographic records boundary-layer velocity profiles were measured for $R_s = 90$ and 400. The measurements were, in effect, all made outside the shear-wave layer and the results were compared with the series solutions, which remain valid at this station. Discrepancies were noted between theory and experiment, particularly in the outer part of the boundary layer. As Bertelsen observed, effects of finite Reynolds number may account for this discrepancy. The purpose of the present paper is to develop the theory of the outer streaming induced by a vibrating cylinder in an unbounded fluid for $R_s \gg 1$ beyond first-order boundary-layer theory in order to assess the effects of finite R_s upon the correlation between theory and experiment. We emphasize at this stage that we are concerned entirely with the induced streaming outside the Stokes shear layer. A summary of the solution within the shear layer may be found, for example, in Stuart (1963).

In §2 we begin by calculating the first-order boundary-layer flow. It is shown that this boundary layer, within which the velocities are $O(1)$, entrains fluid, as of course does the jet which forms along the axis of oscillation. The next step of the procedure is to calculate the mean outer inviscid flow, with velocities $O(R_s^{-\frac{1}{2}})$, for which the cylinder and jet act as a sink of variable strength. The slip velocity, $O(R_s^{-\frac{1}{2}})$, predicted by this inviscid flow at the cylinder surface is corrected by second-order boundary-layer theory. The results predicted by this second-order theory are compared, in §3, with the experimental results of Bertelsen. Qualitatively better agreement between theory and experiment is recorded. However the difference remains sufficiently significant to suggest that effects of finite Reynolds number can account only in part for the discrepancy observed by Bertelsen.

We conclude this section by briefly recalling the theory developed by Riley (1967) for the outer streaming when $R_s = O(1)$. With U_∞, ω^{-1} and a as a typical velocity, time and length respectively the dimensionless stream function in the outer region may be expanded as

$$\psi = \sum_{m=0} \epsilon^m \psi_m(x, y, t, R_s), \tag{1}$$

where (x, y) are Cartesian co-ordinates with origin fixed in the cylinder and all variables are dimensionless. Substitution of (1) into the non-dimensional Navier–Stokes equations yields, to first order,

$$\psi_0 = \psi_{0p}(x, y) \cos t,$$

where $\psi_{0p}(x, y)$ represents the stream function for steady irrotational flow past a cylinder with uniform flow at infinity parallel to the axis of oscillation, say $y = 0$. This inviscid solution yields at the cylinder surface $\tilde{y} = 0$ a slip velocity $V_s(\tilde{x}) \cos t$, which is adjusted in the Stokes shear layer, of thickness $O(\epsilon/R_s^{\frac{1}{2}})$. Here $(\tilde{x}, \tilde{y})$ are orthogonal co-ordinates with $\tilde{y}$ measured normal to the cylinder surface. The $O(\epsilon)$ term in (1) is decomposed as

$$\psi_1 = \psi_1^{(u)}(x, y, t, R_s) + \psi_1^{(s)}(x, y, R_s), \tag{2}$$

where $\psi_1^{(s)}$ represents the time-independent mean motion upon which we wish to focus attention. Riley shows that it is only when the equation for ψ_3 in (1) is considered that the equation for $\psi_1^{(s)}$ emerges. This contains no direct contribution from the Reynolds stresses, and is essentially the full Navier–Stokes equation with R_s as the Reynolds number. Thus

$$\partial(\psi_1^{(s)}, \nabla^2 \psi_1^{(s)})/\partial(x, y) + R_s^{-1} \nabla^4 \psi_1^{(s)} = 0, \tag{3}$$

with

$$\nabla \psi_1^{(s)} = o(1) \quad \text{as} \quad x^2 + y^2 \to \infty, \tag{4a}$$

$$\psi_1^{(s)} = 0, \quad \partial \psi_1^{(s)}/\partial \tilde{y} = -\tfrac{3}{4} V_s dV_s/d\tilde{x} \quad \text{on} \quad \tilde{y} = 0. \tag{4b}$$

The boundary conditions at $\tilde{y} = 0$ arise from the necessity to match $\psi_1^{(s)}$ with the corresponding shear-layer solution.

Equations (3) and (4) form the basis for our discussion of the steady streaming in subsequent sections.

2. The solution for $R_s \gg 1$

For the particular geometry under consideration, namely a circular cylinder, it proves convenient to work in terms not of the co-ordinates (x, y) of §1 but of the plane polar co-ordinates defined in figure 1. Also, for the purpose of developing the solution of (3) for $R_s \gg 1$ it is more convenient to use not (3) but the Navier–Stokes equations in the form

$$\partial u/\partial \theta + \partial(rv)/\partial r = 0, \tag{5}$$

$$\frac{u}{r}\frac{\partial u}{\partial \theta} + v\frac{\partial u}{\partial r} + \frac{uv}{r} = -\frac{1}{r}\frac{\partial p}{\partial \theta} + \frac{1}{R_s}\left(\nabla^2 u + \frac{2}{r^2}\frac{\partial v}{\partial \theta} - \frac{u}{r^2}\right), \tag{6}$$

$$\frac{u}{r}\frac{\partial v}{\partial \theta} + v\frac{\partial v}{\partial r} - \frac{u^2}{r} = -\frac{\partial p}{\partial r} + \frac{1}{R_s}\left(\nabla^2 v - \frac{v}{r^2} - \frac{2}{r^2}\frac{\partial u}{\partial \theta}\right), \tag{7}$$

where $\nabla^2 = \partial^2/\partial r^2 + r^{-1}\partial/\partial r + r^{-2}\partial^2/\partial\theta^2$ and the velocity components are related to $\psi_1^{(s)}$ by $u = \partial\psi_1^{(s)}/\partial r$ and $rv = -\partial\psi_1^{(s)}/\partial\theta$. We choose the typical length a of §1 to be the cylinder radius, so that from (4*b*) $v = 0$ at $r = 1$. The 'slip' boundary condition at $r = 1$ is calculated as follows. For a circular cylinder the slip velocity at the surface predicted by potential flow is $V_s(\theta) = 2\sin\theta$. If we now define

$$\xi = \theta - \tfrac{1}{2}\pi, \tag{8}$$

then we require, from (4*b*),

$$u = \tfrac{3}{2}\sin 2\xi \quad \text{at} \quad r = 1. \tag{9}$$

We see from (8) and (9) that ξ measures distance around the cylinder from the stagnation point S, and since the flow is symmetrical about the lines CC and SS we need only consider the range $0 \leqslant \xi \leqslant \frac{1}{2}\pi$. Finally, the boundary condition (4*a*) requires that $u, v \to 0$ as $r \to \infty$.

Solutions of (5)–(7) of the form

$$\left.\begin{aligned} u &= u_1 + R_s^{-\frac{1}{2}}u_2 + \ldots, \\ v &= R_s^{-\frac{1}{2}}v_1 + R_s^{-1}v_2 + \ldots, \\ p &= R_s^{-\frac{1}{2}}p_2 + \ldots \end{aligned}\right\} \tag{10}$$

are now sought. We remark that outside the boundary-layer region, which itself has thickness $O(R_s^{-\frac{1}{2}})$, $u_1 \equiv 0$, so that we are anticipating in (10) the fact that the first-order inviscid solution in that region vanishes. We now consider the first-order boundary-layer solution, second-order inviscid flow and second-order boundary layer, matching at each stage in turn. For the boundary-layer region we introduce a co-ordinate η defined by

$$r = 1 + R_s^{-\frac{1}{2}}\eta. \tag{11}$$

First-order boundary layer

Substituting (8), (10) and (11) into (5)–(7) gives, retaining terms $O(1)$ and using (9), the following problem for u_1 and v_1:

$$\left.\begin{aligned} \partial u_1/\partial\xi + \partial v_1/\partial\eta &= 0, \\ u_1\partial u_1/\partial\xi + v_1\partial u_1/\partial\eta &= \partial^2 u_1/\partial\eta^2, \end{aligned}\right\} \tag{12}$$

with

$$\left.\begin{aligned} v_1 = 0, \quad u_1 = \tfrac{3}{2}\sin 2\xi \quad &\text{on} \quad \eta = 0, \\ u_1 \to 0 \quad &\text{as} \quad \eta \to \infty, \end{aligned}\right\} \tag{13}$$

together with $u_1 \equiv 0$ on the stagnation line $\xi = 0$. Series solutions of these equations, in odd powers of ξ, were obtained by Riley (1965) and Stuart (1966). These series are of limited value since only a few terms have been calculated. In order to extend the solution up to the axis of oscillation $\xi = \frac{1}{2}\pi$, where the boundary layers originating from the points S in figure 1 collide, Davidson & Riley (1972) used a fully implicit finite-difference technique to solve (12) and (13). Results from this numerical integration for the tangential velocity profile u_1 are shown in figure 2 at angular distances of 30°, 60°, 75° and 90° from S. We note in particular that at $\xi = \frac{1}{2}\pi$ the boundary layer does not become empty, leading to an inevitable collision of the boundary layers as anticipated by figure 1.

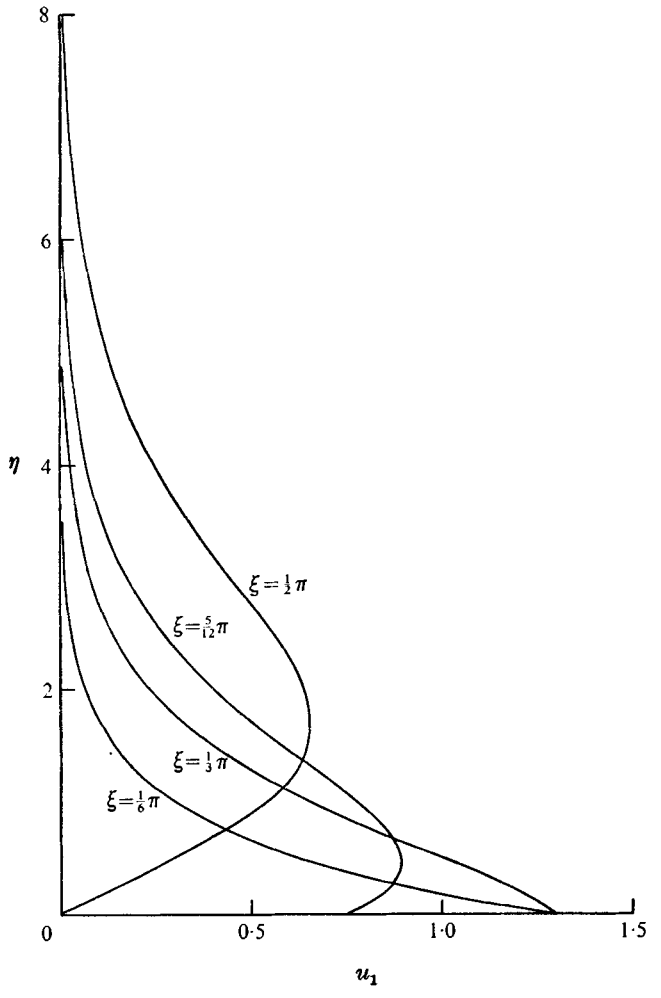

FIGURE 2. The velocity profiles u_1 calculated from first-order boundary-layer theory.

Second-order inviscid flow

From the first-order boundary-layer solution we may calculate $v_{1\infty}$, the value of v_1 at the edge of the boundary layer. This is shown in figure 3, where it is seen to be negative for all ξ. Just as this boundary layer on the cylinder entrains fluid so does the jet, also with entrainment velocity $O(R_s^{-\frac{1}{2}})$. If this entrainment velocity along the axis of oscillation is known, together with that on $r = 1$, then the outer inviscid flow, $O(R_s^{-\frac{1}{2}})$, is due to a known sink distribution along $y = 0$ $(x < -1, x > 1)$ and $r = 1$, and may be calculated using elementary complex-variable methods.

Consider now the jet emerging on the axis of oscillation $y = 0, x > 1$. Davidson & Riley (1972) observed in their experiments that the jet profile had achieved the similarity form predicted by Bickley (1937) within one diameter from the

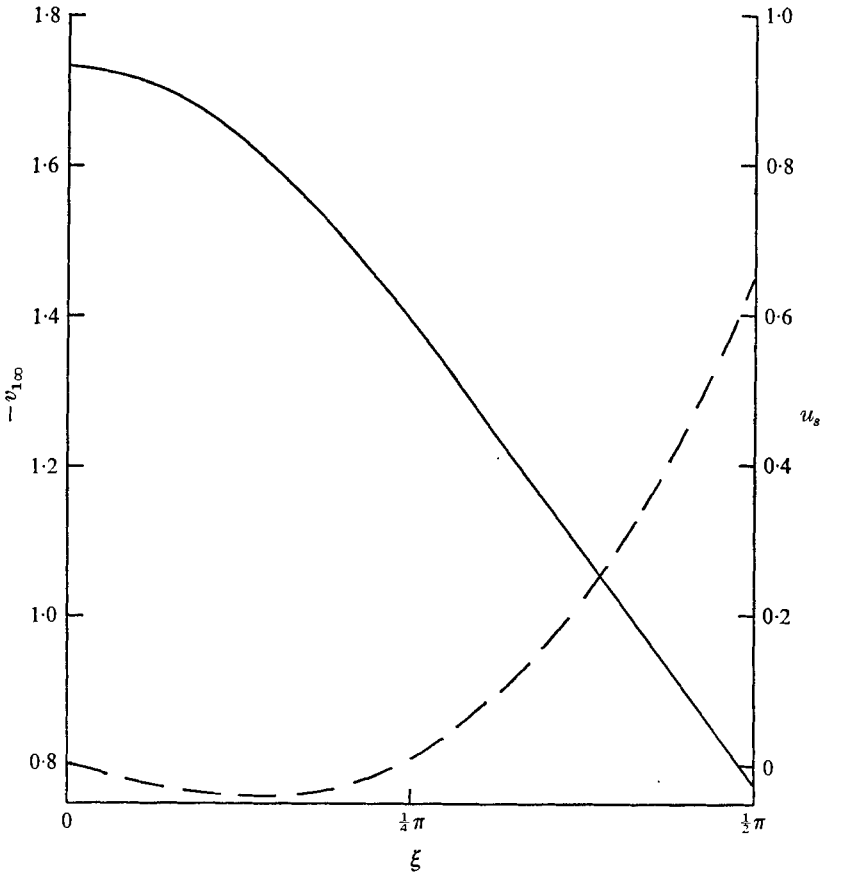

FIGURE 3. The entrainment velocity $v_{1\infty}$ at the outer edge of the boundary layer (——) and the slip velocity u_s at the cylinder surface predicted by the outer inviscid flow (– – –).

point at which the jet emerges. If we adopt Bickleys' similarity solution for the flow in the jet then

$$\left.\begin{aligned} \psi_1^{(s)} &= [\tfrac{9}{2}N(x+x_0)]^{\frac{1}{3}}\tanh\tilde{\eta}, \\ \text{with} \qquad \tilde{\eta} &= (N/48(x+x_0)^2)^{\frac{1}{3}}y, \end{aligned}\right\} \tag{14}$$

where N is the momentum flux in the jet and x_0 is an arbitrary constant which reflects the uncertainty in the location of the origin for the similarity solution. The momentum flux in the jet will be related to the terminal momentum flux

$$M = \int_0^\infty u_1^2|_{\xi=\frac{1}{2}\pi}\,d\eta$$

in the boundary layer on the cylinder. In a region of dimensions $O(R_s^{-\frac{1}{2}})$ centred upon C, neither the cylinder boundary-layer solution nor the jet solution is appropriate. Order-of-magnitude arguments show that the flow in this region is effectively inviscid, so that $\bar{\nabla}^2\psi_1^{(s)} = f(\psi_1^{(s)})$, where $\bar{\nabla}^2$ is the Laplacian operator on the scale of this region. Now, in this region, as we approach either the boundary layer or jet the inviscid equation for $\psi_1^{(s)}$ may be approximated as

$$\partial^2\psi_1^{(s)}/\partial n^2 \approx f(\psi_1^{(s)}),$$

where $n = \eta$ and η_1 in the boundary layer and jet respectively. Consequently we conclude that the velocity profiles at the end of each boundary layer are convected around and emerge essentially unchanged on this scale. Similar situations, but in different physical contexts, have been encountered by Stewartson (1958) and Lyne (1971). Exploiting this result we have $N = 2M = 1{\cdot}928$, where the terminal momentum flux M is obtained from the calculated boundary-layer profile $u_1|_{\xi=\frac{1}{2}\pi}$. To determine x_0 we insist that mass be conserved and equate the mass flux in the jet at $x = 1$ with that in the boundary layers impinging at C. This gives $x_0 = 0{\cdot}1$. Finally, then, we have for the entrainment velocity along $y = 0\,(x > 1)$

$$v_{1\infty} = -0{\cdot}685/(x+0{\cdot}1)^{\frac{3}{2}}. \tag{15}$$

Although the solution (14) cannot be expected to describe the details of the flow in the jet close to C, we consider that (15) is an accurate representation of the entrainment velocity along $y = 0$ $(x > 1)$. A similar expression gives the entrainment velocity along $y = 0$ $(x < -1)$.

We are now in a position to calculate those quantities associated with the outer inviscid flow which are of direct interest to us. First we transform the plane $z = re^{i\theta} = x+iy$ to the complex Z plane via the elementary transformation

$$Z = z+z^{-1} = X+iY, \tag{16}$$

so that the circle $r = 1$ is transformed to the slit $-2 < X < 2$, $Y = 0$ and the axis of oscillation $y = 0$, $x > 1$, $x < -1$ to the slit $|X| > 2$, $Y = 0$.

The velocity components in the physical plane with which we are concerned at this stage are denoted by $(R_s^{-\frac{1}{2}}U_2, R_s^{-\frac{1}{2}}V_1)$ in the transformed plane. Of prime concern to us in our study of the boundary layer on the cylinder is the slip velocity predicted at the surface; this is given by

$$u_s = 2U_2(X, 0)\sin\theta, \tag{17}$$

with

$$U_2(X, 0) = \frac{1}{2\pi}\int_{-\infty}^{\infty} \frac{q(s)\,ds}{X-s}, \tag{18}$$

where the Cauchy principal value in (18) is to be understood. The source strength $q(X) = 2V(X, 0+)$ per unit length has, by symmetry, the property $q(-X) = q(X)$, so that, after a little manipulation, (18) may be written as

$$U_2(X, 0) = \frac{X}{\pi}\int_0^{\infty} \frac{q(s)\,ds}{X^2-s^2}. \tag{19}$$

Since the source strength is invariant under the transformation (16) we calculate $q(X)$ as

$$q(X) = \begin{cases} 2v_{1\infty}/(4-X^2)^{\frac{1}{2}}, & X < 2, \qquad (20a) \\ 2v_{1\infty}\dfrac{X^2+X(X^2-4)^{\frac{1}{2}}-2}{(X^2-4)^{\frac{1}{2}}\{X+(X^2-4)^{\frac{1}{2}}\}}, & X > 2, \qquad (20b) \end{cases}$$

where in (20a) $v_{1\infty}$ is deduced from the first-order boundary-layer calculation as shown in figure 3, and in (20b) $v_{1\infty}$ is derived from (15).

The slip velocity at the cylinder surface predicted from the second-order outer inviscid flow by (17) and (18), which provides an outer boundary condition for

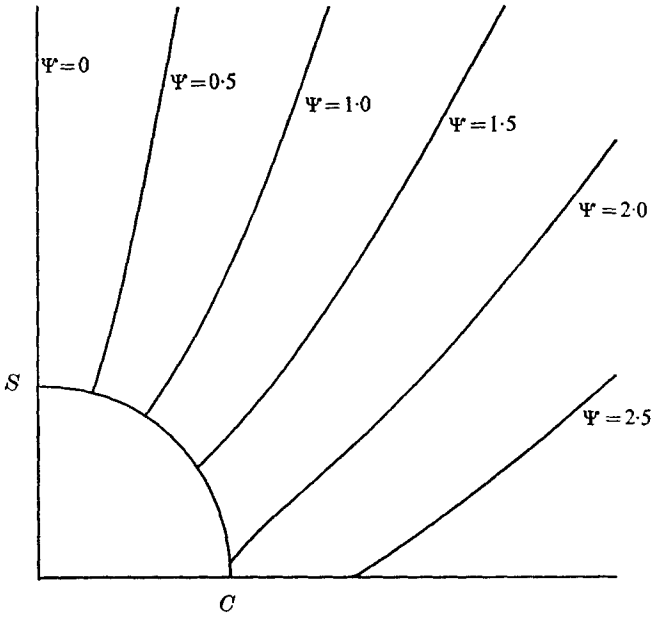

FIGURE 4. The streamline pattern associated with the outer inviscid flow $O(R_s^{-\frac{1}{2}})$.

the second-order boundary layer, is shown in figure 3. In the absence of the sink distribution due to the jet we have a variable sink strength at the cylinder surface due to the entrainment velocity shown in figure 3. The strength decreases as θ increases and this in turn implies a slip velocity at the cylinder surface from C to S. This trend is discernible in figure 3 for u_s but is counteracted as C is approached by entrainment into the jet.

The streamline pattern associated with the outer inviscid flow, $O(R_s^{-\frac{1}{2}})$, is calculated from

$$\Psi(X, Y) = \frac{1}{2\pi}\int_{-\infty}^{\infty} q(s)\tan^{-1}\left(\frac{Y}{X-s}\right)ds, \tag{21}$$

where Ψ is the stream function for the inviscid flow, $O(R_s^{-\frac{1}{2}})$, in the transformed plane. The streamlines obtained from (21) and (16) are shown, in the neighbourhood of the cylinder, in figure 4. When u_s is close to zero the streamlines approach the cylinder normally. However as C is approached and u_s increases the streamlines meet the cylinder at an increasing angle to the normal, as shown in figure 4. We note also that for an unbounded fluid domain all the streamlines entering the jet do so 'backwards'.

Second-order boundary layer

The slip velocity u_s at the cylinder surface predicted by the outer flow is accommodated by the second-order boundary-layer calculation. We now substitute (10) and (11) into (5)–(7) and select the terms $O(R_s^{-\frac{1}{2}})$. From the continuity equation (5) we have

$$\frac{\partial u_2}{\partial \xi} + \frac{\partial v_2}{\partial \eta} = -\frac{\partial}{\partial \eta}(\eta v_1). \tag{22}$$

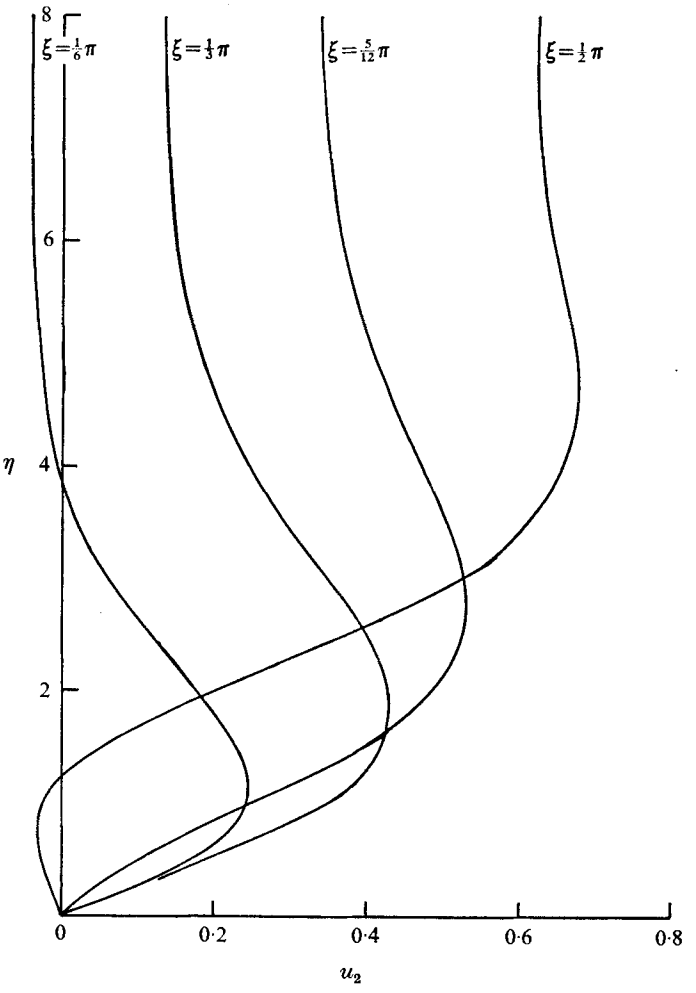

FIGURE 5. Profiles of u_2 resulting from the second-order boundary-layer calculation.

The radial momentum equation (7) shows that pressure variations across the boundary layer are given by

$$\partial p_2/\partial \eta = u_1^2, \tag{23}$$

and substituting for p_2 from (23) in the transverse momentum equation (6) gives

$$u_2\frac{\partial u_1}{\partial \xi}+u_1\frac{\partial u_2}{\partial \xi}+v_2\frac{\partial u_1}{\partial \eta}+v_1\frac{\partial u_2}{\partial \eta}-\frac{\partial^2 u_2}{\partial \eta^2}=\frac{\partial}{\partial \xi}\int_\eta^\infty u_1^2\,d\eta+\frac{\partial u_1}{\partial \eta}+\tfrac{1}{2}\eta\frac{\partial}{\partial \xi}(u_1^2)-u_1v_1. \tag{24}$$

Equations (22) and (24) are solved, using the implicit finite-difference scheme referred to earlier, subject to the boundary conditions

$$\left.\begin{aligned} &u_2 = v_2 = 0 \quad \text{on} \quad \eta = 0,\\ &u_2 \to u_s \quad \text{as} \quad \eta \to \infty, \end{aligned}\right\} \tag{25}$$

together with the initial condition $u_2 \equiv 0$ at $\xi = 0$. In figure 5 profiles of u_2 are shown. Two factors dominate the distribution of u_2: the term representing the pressure gradient in (24) and the velocity u_s at the outer edge of the boundary layer. Initially the pressure gradient is favourable with a small reversed flow at the edge of the boundary layer. The velocity at the edge of the boundary layer gradually increases as shown in figure 3 whilst, in fact, the pressure gradient becomes adverse, leading eventually to a distribution of u_2 which has negative values close to the boundary. These features are illustrated in figure 5.

3. Discussion of results

In this section we discuss the experimental results of Bertelsen in relation to the theoretical predictions of § 2.

As we have already mentioned in § 1 the experimental technique of Bertelsen enabled him to measure velocity profiles in the boundary layer on the cylinder. The experimental profiles which he presents are at approximately 57° from the stagnation point S, and all the measurements were made outside the shear-wave layer. The two sets of results presented are for $\epsilon = \frac{1}{24}, R_s = 90$ and $\epsilon = \frac{1}{20}, R_s = 400$, and we note that Bertelsen bases ϵ upon the diameter, not the radius, of the cylinder. Since, for these experiments, ϵ and $R_s^{-\frac{1}{2}}$ are comparable we observe that any contributions to the time-independent velocity parallel to the surface in addition to those from the series (10) are at most $O(\epsilon^2 R_s^{-\frac{1}{2}})$ and therefore smaller than those $[O(\epsilon R_s^{-\frac{1}{2}})]$ which have been retained in our outer solution. Bertelsen's results are shown in figure 6 together with theoretical curves from both first- and second-order boundary-layer theory, with $R_s = 90$ for the latter. In figure 6 the theoretical curves are of course the mean Eulerian velocity profiles; as Bertelsen observes, the Stokes drift becomes insignificant outside the shear-wave layer. Figure 6 shows that when effects of finite Reynolds number are taken into account the agreement between theory and experiment is improved but, at best, we can still only claim qualitative agreement. As far as the experimental results themselves are concerned (the presentation here differs from the normalized plots of Bertelsen's figure 6, where the abscissa should be $(r-a)/\delta_s$) such trends as are discernible as R_s increases could possibly be accounted for by the effects of finite R_s.

The only other detailed experimental measurements at high values of R_s have been made by Davidson & Riley (1972). Their measurements are of the flow in the jet which emerges along the axis of oscillation, for values of $R_s \approx 300$. They obtain relatively good agreement between the measured and theoretical values for the momentum flux in the jet using first-order boundary-layer theory, which, to some extent, substantiates the model of jet entrainment adopted here. Although the momentum flux in the jet is a gross property of the flow the agreement referred to above suggests that the discrepancy between theory and experiment in the present case must owe its origin to effects other than finite R_s.

In the experiments the ratio A/a of the radius of the containing cylinder to that of the vibrating cylinder varied between 13 and 20. Although Bertelsen considers that in his experiments the finite size of the container cannot explain

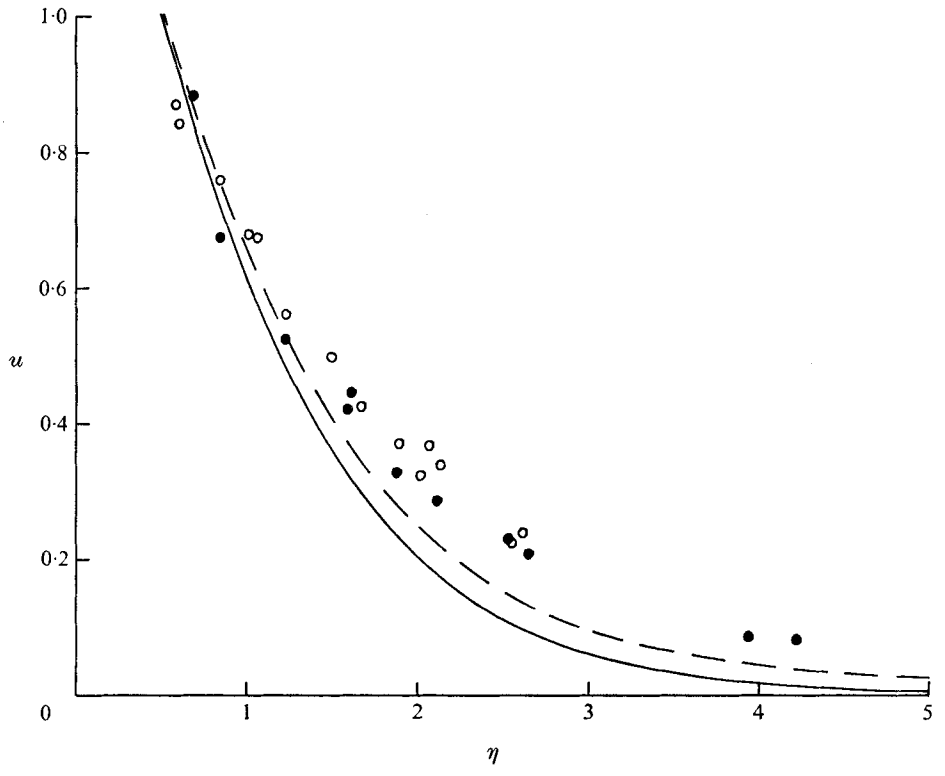

FIGURE 6. Comparison between first-order boundary-layer theory (solid line) and second-order boundary-layer theory at $R_s = 90$ (dashed line), with the experimental measurements of Bertelsen (1974) for $R_s = 90$ (open circles) and $R_s = 400$ (solid circles) at $\xi \approx 1$.

the observed discrepancy, this point is worthy of further consideration. When the cylinder begins to vibrate from a state of rest with frequency ω the time which elapses before the Stokes shear wave is established is $O(\omega^{-1})$. We note that in the experiments the range of frequencies was 150–350 Hz. It has been shown by Riley (1967) that the outer boundary layer develops over the much longer time scale $O(\epsilon^{-2}\omega^{-1})$. This also corresponds to the time taken for the jet, in which the velocities are $O(\epsilon U_\infty)$, to become established. At this stage we have a quasi-steady flow away from the immediate neighbourhood of the outer containing cylinder which is independent of its size. Outside the boundary layer on the vibrating cylinder and the jet we shall have irrotational flow and the theory of §2 is directly applicable. However, because of the presence of the outer container we cannot expect this situation to prevail for all time. The fluid velocities outside the boundary layer and jet are $O(\epsilon R_s^{-\frac{1}{2}} U_\infty)$, and so the time taken for a fluid particle to traverse the finite distance between the two cylinders will be $O(R_s^{\frac{1}{2}}\epsilon^{-2}Aa^{-1}\omega^{-1})$. After that time we can expect the effects of the outer cylinder to be important. For example, it seems likely that there will be regions of recirculating flow in which, according to the Prandtl–Batchelor theorem, the vorticity will be uniform. These regions of flow with uniform vorticity can be

expected to lead to significant modifications to the results derived in §2 for an unbounded fluid region.

In the presentation of his experimental results Bertelsen does not indicate the time which had elapsed from the initiation of the motion before the measurements were made. An examination of figure 4(*a*) (plate 1) in Bertelsen's paper shows that the outer inviscid flow, inferred from the experiments, will have a stagnation point on the jet axis between one and two diameters from the inner cylinder surface. We recall that the results of §2 show that when the fluid region is unbounded the streamlines always enter the jet backwards. This suggests that in the experiments a sufficient time had elapsed following the initiation of the motion for the effects of the outer containing cylinder to be important close to the vibrating cylinder.

Another possible explanation for the difference between theory and experiment advanced by Bertelsen is the upstream effect of 'separation' where the boundary layers erupt at the points C. However Davidson & Riley did not observe separation, in the conventional sense, at C in their experiments and as we have indicated in §2, the region in which the boundary layers turn to form the jet is one of size $O(aR_s^{-\frac{1}{2}})$.

We may conclude that the effects of a finite R_s explain only in part the discrepancy observed by Bertelsen between experiment and first-order boundary-layer theory. The effects of the outer container appear to be comparable with those of finite R_s in the experiments and further work, of either a theoretical or experimental nature, is necessary to explain fully the discrepancies observed by Bertelsen between theory and experiment.

The author is indebted to Professor J.T. Stuart and Professor D. W. Moore for their constructive criticisms and comments upon an earlier version of this paper.

REFERENCES

Bertelsen, A. F. 1974 *J. Fluid Mech.* **64**, 589.
Bickley, W. G. 1937 *Phil. Mag.* **23**, 727.
Davidson, B. J. & Riley, N. 1972 *J. Fluid Mech.* **53**, 287.
Longuet-Higgins, M. S. 1953 *Phil. Trans.* A **245**, 535.
Lyne, W. H. 1971 *J. Fluid Mech.* **45**, 13.
Riley, N. 1965 *Mathematika*, **12**, 161.
Riley, N. 1967 *J. Inst. Math. Appl.* **3**, 419.
Stewartson, K. 1958 In *Proc. Symp. b.l. Res. Frieburg i Br.* 1957, pp. 57–91. Springer.
Stuart, J. T. 1963 *Laminar Boundary Layers*, chap. 7. Oxford University Press.
Stuart, J. T. 1966 *J. Fluid Mech.* **24**, 673.